Article

Not peer-reviewed version

The Effect of Doping rGO with MnO_2 Nanomaterial on Its Gas Sensing Properties

Mohamed Ayoub Alouani , Juan Casanova-Chafer , Santiago de Bernardi-Martín , Alejandra García-Gómez , Foad Salehnia , José Carlos Santos-Ceballos , Alejandro Santos-Betancourt , Xavier Vilanova * , Eduard Llobet *

Posted Date: 22 October 2024

doi: 10.20944/preprints202410.1611.v1

Keywords: reduced graphene oxide; manganese dioxide (MnO2); gas sensor; NO2 detection; NH3 detection

Article

The Effect of Doping rGO with MnO_2 Nanomaterial on Its Gas Sensing Properties

M.A. Alouani [1,2,3], J. Casanova-Chafer [4], S. de Bernardi-Martín [5], A. García-Gómez [5], F. Salehnia [1,2,3], J.C. Santos-Ceballos [1,2,3], A. Santos-Betancourt [1,2,3], X. Vilanova [1,2,3,*] and E. Llobet [1,2,3,*]

1 Universitat Rovira i Virgili, MINOS, School of Engineering, Avda. Països Catalans 26, 43007 Tarragona, Spain
2 IU-RESCAT, Research Institute in Sustainability, Climatic Change and Energy Transition, Universitat Rovira i Virgili, Joanot Martorell 15, 43480 Vila-seca, Spain
3 TecnATox - Centre for Environmental, Food and Toxicological Technology, Universitat Rovira i Virgili, Avda. Països Catalans 26, 43007 Tarragona, Spain
4 Université de Mons, Place du Parc 23, 7000 Mons, Belgium
5 Gnanomat. C/Faraday 7, 28049 Madrid, Spain
* Correspondence: xavier.vilanova@urv.cat (X.V.); eduard.llobet@urv.cat (E.L.)

Abstract: Manganese dioxide (MnO_2) has drawn attention as a sensitizer to be incorporated in graphene-based chemoresistive sensors thanks to its promising properties. In this regard, a rGO@MnO_2 sensing material was prepared and deposited on two different substrates (Silicon and Kapton). These sensors were exposed to different dilutions of NO_2 under dry and humid conditions at room temperature. Other gases or vapours such as NH_3, CO, ethanol and H_2 were also tested. FESEM, HRTEM, RAMAN and XRD were used to characterize the prepared sensors. The experimental results showed that the incorporation of MnO_2 in the rGO material enhanced its response towards NO_2. Moreover, this material showed also very good responses toward NH_3 both under dry and humid conditions and showed no cross-responsiveness towards other toxic gases.

Keywords: reduced graphene oxide; manganese dioxide (MnO_2); gas sensor; NO_2 detection; NH_3 detection

1. Introduction

Technological and economic advances increasingly threaten the environment and air quality, necessitating urgent solutions. The demand for low-cost and effective gas sensors, crucial for detecting toxic agents such as nitrogen dioxide NO_2 [1], ammonia NH_3 [2], and carbon monoxide CO [3] in various fields, has never been more pressing. While traditional methods like infrared spectrophotometry (IRSP) [4], non-dispersive infrared analysis (NDIR) [5], and gas chromatography-mass spectrometry (GC-MS) [6] have been widely used for detecting toxic gases, they are not without significant drawbacks. Their high cost and complexity have underscored the need for a new, more efficient approach. This realization has led to the development of chemoresistive devices, known for their ease of operation, low production cost, fast response time, and ease of miniaturization [7].

Since their first use in the 1960s, metal oxides (MOX) such as ZnO [8], SnO_2 [9], WO_3 [10], and many more [11] have been studied as sensitive films to be used in the fabrication of chemoresistive devices for gas sensing and especially for detecting NO_2. Even though MOX are effective and sensitive, the need for a pervasive, widespread monitoring of air pollutants, has oriented research to the discovery of new, less power-hungry, gas sensitive materials. This has, for example, led to the emergence of graphene-based chemoresistive sensors. The unique and exceptional properties of graphene that made it a solid gas sensing material candidate are thermal stability, mechanical robustness, high conductivity, high carrier mobility at low to room temperatures, a large surface area of up to 2630 m^2/g for single-layer graphene, low electrical noise [12] and, most importantly, the fact that its electronic properties are easily affected by the adsorption of gas molecules [13].

 doi:10.20944/preprints202410.1611.v1

One of the graphene derivatives is reduced graphene oxide (rGO). It was reported in the literature to be the best and most used graphene-based sensing material for detecting NO_2 [14] and NH_3 [15] due to its numerous defect sites and functional groups, which facilitate gas adsorption. rGO has been reported able to detect chemical warfare agents and explosives at trace levels (ppb) [16]. Moreover, the synthesis of rGO can be achieved via straightforward and inexpensive processes that reduce GO via chemical and thermal routes or even using UV light [17]. Studies have shown that pristine rGO gas sensors exhibit slow response and recovery dynamics. Hence, the hybridization of rGO with MOx has been a solution often explored to enhance its sensing properties (e.g. ameliorating response dynamics and extending the number of gases that can be detected), D.Tripathi et al, explored this process and an enhancement of the sensitivity and selectivity of the rGO material towards ammonia by incorporating WO_3 nanomaterial in the sensing layer was achieved [18]. Another reported work of D. Milad et al, where they showed that the synthesis of a TiO_2/rGO composite exhibited an improved gas sensing properties towards methanol and ethanol [19]. This is achieved via the MOX nanoparticles supported on rGO behaving as catalysts or as electronic sensitizers, favouring the occurrence of heterojunctions at the MOX/rGO interface.

Some of the reported MOx nanoparticles used for the loading of the rGO layers for gas sensing are ZnO [20], SnO_2 [21], and WO_3 [22]. Still, in recent years, MnO_2 has gained popularity due to its low toxicity, low cost, high stability, and ease of fabrication. It was also used in a wide range of applications and fields such as energy storage [23], biomedical field [24], and in developing gas sensors [25]. However, in the gas sensing field, there is a limited amount of reported work discussing the incorporation of the MnO_2 nanomaterial into rGO to achieve a sensitive layer towards different toxic gases. One of the few works reported is of Hui Zhang et al., where they successfully synthesized an rGO-coated Ni foam-supported MnO_2 for the enhanced detection of NO_2 at a concentration of 50 ppm while the sensor was operated at room temperature [26]. Meanwhile, Alexander et al. modified rGO with doping of MnO_2 nanoparticles and tested the rGO/MnO_2 composite as gas sensor for different gases such as 25 ppm of NO_2, 500 ppm of H_2 and 1000 ppm of CH_4 under dry conditions with heating at 85 °C [27]. Another reported work was of Ghosal et al. where they prepared different hybrids for alcohol vapor detection, being one of the hybrids rGO/MnO_2 nanoflowers binary composite and it showed good responses towards ethanol and methanol vapours in the range of 5-100 ppm while heating at 150 °C [28]. Lastly, Ahmad et al. made a ternary nanocomposite of PANI@rGO@MnO_2 using a multi-step process for NH_3 detection. The tests were made at 100 °C under dry conditions [29]. The fact that very few works have been reported on rGO@MnO_2 gas sensors so far, makes exploring further its gas sensing properties interesting and worthwhile.

In this paper, rGO@MnO_2 sensitive layers were successfully synthesized and deposited on different transducing substrates (Kapton and silicon with gold electrodes). The gas sensing performance of the rGO@MnO_2 sensors was studied for different reducing and oxidizing species. The effect of ambient moisture on sensor response was evaluated as well. Results are presented and thoroughly discussed. A sensing mechanism for the detection of ammonia and nitrogen dioxide is presented.

2. Materials and Methods

In this section a detailed explanation of the preparation of the doped reduced graphene oxide with MnO_2 nanomaterial with 95/5 wt.% alongside the process of depositing it on the Kapton and silicon substrates via the spray coating technique is presented. The section also describes the techniques employed in the study of the morphology and composition of the hybrid material and in the test of its gas sensing properties.

2.1. Preparation of Reduced Graphene Oxide Doped with MnO_2

rGO doped with MnO_2 nanomaterial (rGO/MnO_2 95/5 wt.%) was synthesized using a process based on patented procedures (Patent number ES2678419A1). Briefly, reduced graphene oxide was dispersed in oxalic acid, in which the starting Mn_3O_4 had been previously dissolved at 50 °C. After homogenization, MnO_2 nanomaterials were slowly precipitated on reduced graphene oxide by

 doi:10.20944/preprints202410.1611.v1

adding a basic solution (NaOH 5 M) under vigorous agitation. The solid was filtered and dried at 90 °C overnight. Synthesis parameters such as temperature, stirring speed, addition rate, or MnO_2/rGO proportion, were controlled to obtain the desired crystallinity that provides the material the optimal properties. Manganese oxide phase was checked via XRD, Figure S1 (in Supplementary Materials) shows the XRD diffractogram.

2.2. Substrates Preparation and Material Deposition

10 mg of the rGO@MnO_2 nanomaterial were weighted and suspended in a 10 ml ethanol solution via a 30-min sonication. Subsequently, suspended nanomaterials were deposited by spray coating onto two different substrates (i.e., silicon, and Kapton). During the coating process, substrates were heated at 50 °C to promote the evaporation of the solvent and the formation of a homogeneous film. The interdigitated gold electrodes were deposited on the substrates using different processes. For Kapton substrates, 9 nm of gold were sputtered using a shadow mask to form the electrodes. In contrast, for the silicon substrates, a two-step approach took place. At first, a laser lithography technique **(DWL 66fs, Heildelberg Instruments)** was used to pattern a photoresist that coated an oxidized silicon wafer in the shape of the electrodes. In the second step, a titanium adhesion layer was sputtered with a thickness of 10 nm, and then a gold layer was sputtered on top with a thickness of 100 nm. A final lift off process was conducted to obtain the electrodes. The silicon wafer was then diced. Figure 1 shows two sensors on the two types of substrates used.

Figure 1. Pictures of the prepared sensors on the (a) Silicon substrate, (b) kapton substrate.

2.3. Material Characterization and Gas Sensing Measurements

The obtained sensors were characterized using different techniques, such as Raman via a Raman spectrometer (Renishaw, plc., Wotton-under-Edge, UK), with a laser wavelength of 514 nm to check the crystallinity of the materials. A Field Emission Scanning Electron Microscope (FESEM) using a Carl Zeiss AG-Ultra 55 (ZEISS, Jena, Germany) to study the surface morphology and to check the distribution of the nanomaterial on the graphene layer. A JOEL F200 TEM ColdFEG operated at 200 kV was used for the high-resolution transmission electron microscopy (HRTEM) characterization. TEM images and electron diffraction patterns were acquired with a Gatan OneView camera, a CMOS-

 doi:10.20944/preprints202410.1611.v1

based and optical fibre-coupled detector of 4096 by 4096 pixels. Gatan Digital Micrograph program was used to process the (S)TEM images. STEM images (1024 x 1024 pixels) were recorded from the JEOL bright-field (BF) and high-angle annular dark-field (HAADF) detectors with a camera length of 200 mm. Samples were inserted in a JEOL beryllium double-tilt holder for energy-dispersive X-ray spectroscopy (EDS). STEM-EDS mapping was recorded from an EDS Centurio detector (silicon drift) with an effective area of 100 mm^2 and 133 eV of energy resolution. STEM-EDS maps (512 x 512 pixels) were processed with the JEOL Analysis software to check the shape of the MnO_2 nanomaterial and its incorporation in the graphene layers. Gas sensing measurements were conducted by placing the different sensors in an airtight Teflon chamber with a volume of 35 cm^3. A continuous stream of dry air (Air Premier, 99.995% purity) and diluted gases were passed through the testing chamber with a 100 mL/min flow via a set of Bronkhorst mass-flow controllers. The target gases from calibrated bottles (NO_2-1 ppm, CO-100 ppm, NH_3-100 ppm, and ethanol-20 ppm balanced in dry air) were further diluted using the mass flow controllers set. The resistance changes were continuously acquired using an Agilent HP 34972A multimeter. The humidity effect on the sensing performance was assessed by humidifying the gas stream through a controller evaporator mixer (CEM) to obtain low humidity levels of maximum 50% RH at 25ºC. For higher values of relative humidity, the flow of the dry air with the corresponding concentration of gas was humidified passing through a bubbling water system at room temperature. The sensing responses were calculated using the formula $R\ (\%) = ((R_g - R_a)/R_a) \times 100$, where R_g and R_a correspond to the resistance level after and before gas exposure, respectively.

3. Results

This section, presents and discusses at first the results of the characterization tests made for the prepared sensitive layers (rGO and rGO@MnO_2), which are based on the RAMAN, FESEM and HRTEM techniques. Secondly, the gas testing results for these sensors towards NO_2 and NH_3 at room temperature under dry conditions are presented, which is followed by the results gathered at different humidity levels. Additionally, selectivity tests are reported. The results of the gas sensing tests are compared to those found in the literature. Finally, a sensing mechanism for the detection of NO_2 and NH_3 is introduced.

3.1. Sensitive Layer Characterization

3.1.1. Raman

The study of the molecular structure of carbon products and the assessment of disorders and defects in the material can be done using Raman spectroscopy analysis. Two specific peaks always appear when analysing graphene: the G-band and the D-band. The first one, placed at around 1500 cm^{-1}, corresponds to the first-order scattering of the E_{2g} phonons at the Brillouin zone centre and originates from the in-plane vibrations of the sp^2 carbon atoms [30]. Meanwhile, the D-band is observed around 1300 cm^{-1} and represents the formation of j-point photons of A_{1g} symmetry; it is also associated with double bonds C=C, meaning the more intense the band is, the higher the presence of sp^2 domains is. Furthermore, D-band peak intensity depends highly on the presence of disorders and defects like vacancies and edges in the carbon lattice and grain boundaries [31]. To determine the degree of oxidation of the graphene, a simple calculation of the intensity ratio of both the D and G band peaks is enough, i.e., ID/IG; the higher this ratio is, the lower the oxidation level is [32].

Finally, the second-order bands are observed from 2500 cm^{-1} to 3200 cm^{-1}, containing one always visible peak at around 2700 cm^{-1}, known as the 2D band. They are used generally to determine the layers of the graphene since graphene is susceptible to stacking [33]. The chosen name of this band comes from the fact that it is the overtone of the D band, and two of the same phonons responsible for the D band are involved in the 2D band. Two other bands are sometimes reported when studying graphene Raman spectra, which are the D+G band, that can be seen around 2900 cm^{-1}, and the combined overtone of the D and G bands, the 2G band around 3200 cm^{-1}, which is attributed to the overtone of the G band [34]. In our case, we are working with rGO, which means that the stacking of

 doi:10.20944/preprints202410.1611.v1

the layers is random, and since the width of the peaks is relative to the disorder, that can lead to an overlapping of the 2D band peak with the D+G and 2G, resulting in a bump like peak observed in the range of 2600 cm^{-1} to 3100 cm^{-1} [35].

Figures 2a and 2b show the Raman spectra of bare rGO and rGO doped with MnO_2 nanomaterial, respectively. For both cases, D bands are located at 1355 cm^{-1} and G bands around 1590 cm^{-1}. For the second-order bands, three visible peaks corresponding to the 2D, D+G, and 2G bands at respectively 2697 cm^{-1}, 2940 cm^{-1}, and 3188 cm^{-1} are present in the Raman spectra of the reduced graphene oxide; meanwhile, in the Raman spectra of the MnO_2 doped reduced graphene oxide we observe a bump-like peak around 2926 cm^{-1}, which is in agreement with the explanation made previously. Moreover, the ID/IG intensity ratio is 0.89 for rGO@MnO_2 and 0.85 for rGO, showing a slightly lower oxidation level in the doped rGO and the presence of higher number of defects, that can be caused by the doping process. Finally, it was noticed that the Raman signal in the rGO@MnO_2 sample shows a higher intensity than the pristine rGO sample, which can be correlated to the presence of the MnO_2 nanomaterial, since the presence of MOX usually leads to this increase in the intensity [36].

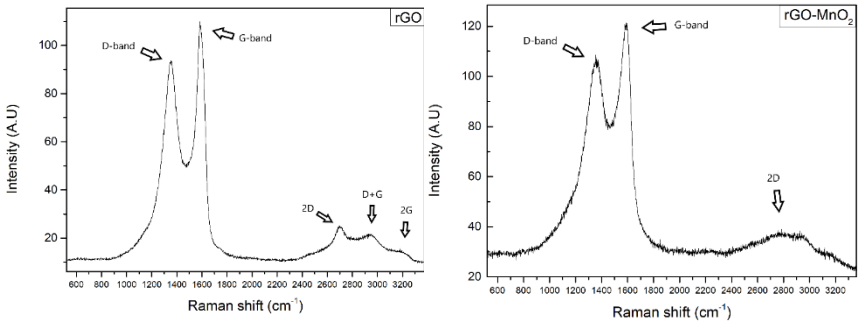

(**a**) (**b**)

Figure 2. (a) Raman spectra of rGO and (b) Raman spectra of rGO@MnO_2.

3.1.2. FESEM

Figure 3.a. shows the obtained FESEM images of the layers present on the surface of the graphene loaded with MnO_2 on the silicon substrate using a back-scattered electron detector (BSE). A very homogenous layers is observed covering the totality of the surface inspected. MnO_2 cannot be clearly seen, even when using a BSE detector, because of the low concentration of the nanomaterial and the small size but, when performing an EDS analysis of the surface, its presence was detected (see Figure s2 in the supplementary materials). Figure 3.b shows the FESEM image of the graphene doped with MnO_2 deposited on Kapton. Again, a very good coverage of the substrate surface is seen. However, in this case the surface of the substrate is getting rapidly charged because of the effect of the magnetic field coming from the BSE detector, leading to the formation of very bright areas. Similarly to the samples on silicon, an EDS analysis (see Figure s3 in the supplementary materials), the presence of MnO_2 was detected on the samples deposited over Kapton. Still, the MnO_2 crystals are too small to be seen in the FESEM images, just as for the sensing layer deposited on silicon.

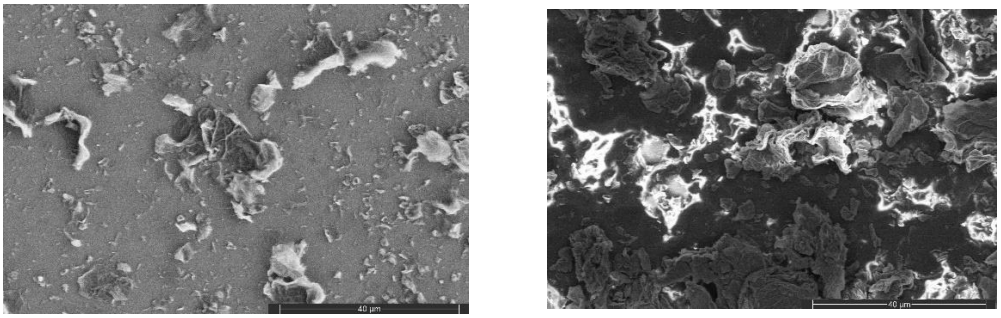

(**a**) (**b**)

 doi:10.20944/preprints202410.1611.v1

Figure 3. FESEM images of (a) the surface of the graphene doped with MnO_2 deposited on the Silicon substrate and (b) the surface of the graphene doped with MnO_2 deposited on the Kapton substrate.

3.1.3. HRTEM

An HR-TEM analysis was conducted to examine better the morphology of the MnO_2 nanomaterial and its incorporation in the graphene layer. Figure 4 shows an HR-TEM image of layers of graphene in addition to an interesting structure on the top right side; zooming in on this structure (Figure 4.b), a sponge-like shaped nanomaterial was observed, which was attributed to the MnO_2 after performing an EDS analysis. Moreover, when chemically mapping the chosen area's surface, a high concentration of Mn is located in the same position as the sponge-like structure, proving the presence and the likely shape of the MnO_2 nanomaterial. Figure 4.d shows an EDS map spectrum of the same area, showing the elements present in the mapping appearing Mn with the highest concentration; the other elements, except for C and O, come from the grid of the HRTEM.

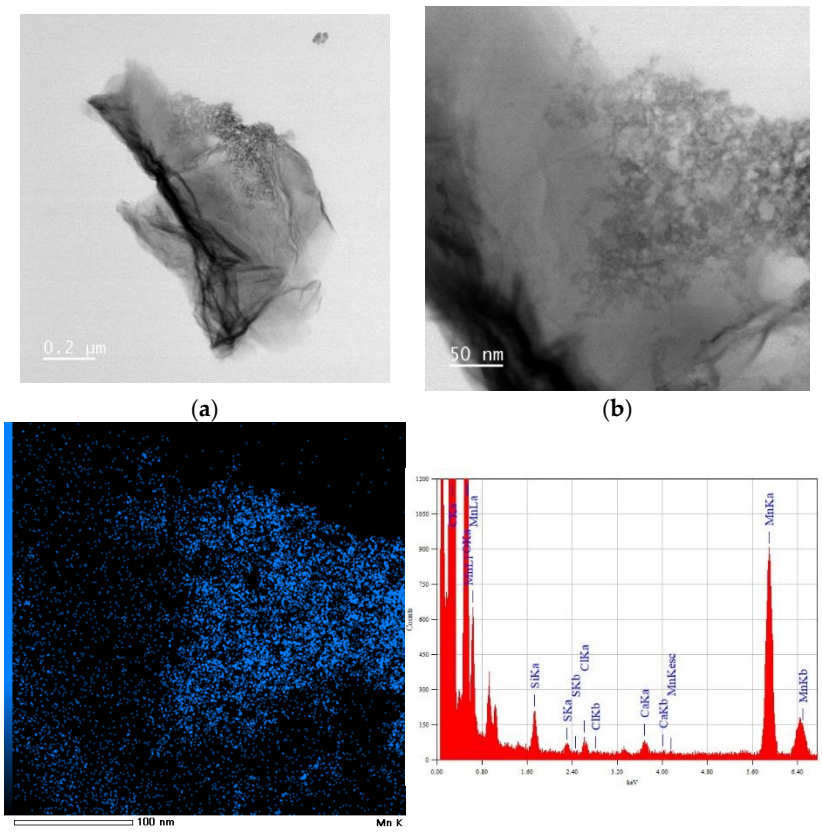

(**a**) (**b**) (**c**) (**d**)

Figure 4. (a) HRTEM image of layered graphene doped with MnO_2 nanomaterial (b) a zoomed HRTEM image of a scale of 50 nm of the same material (c) EDS mapping showing Mn concentration on the area of analysis (d) EDS map spectrum of the studied area.

3.2. Gas Sensing Results

A selection of different toxic gases and vapours was used to study the sensing properties of the pristine rGO and rGO@MnO_2 sensors. First, NO_2 was thoroughly studied with different dilutions ranging from 200 ppb up to 1000 ppb under dry air as well as under ambient moisture conditions (close to real conditions). Sensors were always operated at room temperature. Then, NH_3 was also tested as an interferent gas with a concentration of 50 ppm under the same conditions used for NO_2. Figure 5.a shows the response of the different sensors towards different concentrations of NO_2. It was noticed that the type of substrate used does not affect the response of the sensitive layer towards the analyte. rGO on silicon and Kapton have almost the same response through the studied range, with an average difference of 0.8%. The same behaviour was also seen for the rGO@MnO_2 sensors, where

 doi:10.20944/preprints202410.1611.v1

the average difference between the responses was 0.4%. Moreover, the most important aspect to notice is that the sensors based on rGO incorporating MnO_2 show a superior response than the pristine ones (2-fold increase in response). The loading of rGO with MnO_2 is effective at increasing sensitivity towards NO_2. In fact, rGO@MnO_2 on Kapton exhibits a higher sensitivity of 3 % ppm^{-1} compared to the 1 % ppm^{-1} for the pristine rGO, meanwhile for the materials deposited on silicon the sensitivity of the doped material is slightly better than its pristine counterpart with 1.8 % ppm^{-1} for rGO@MnO_2 on silicon and 1.5 % ppm^{-1} for on rGO silicon. The sensitivity values were evaluated from the slope of the line obtained from the linear regression of the responses of the sensor towards different concentrations of the gas. Figure 5.b shows the resistance changes of the rGO@MnO_2 on silicon substrate for 600 ppb of NO_2 and Figure 5.c shows the resistance changes of the rGO@MnO_2 on Kapton substrate for 600 ppb of NO_2 at 25% RH.

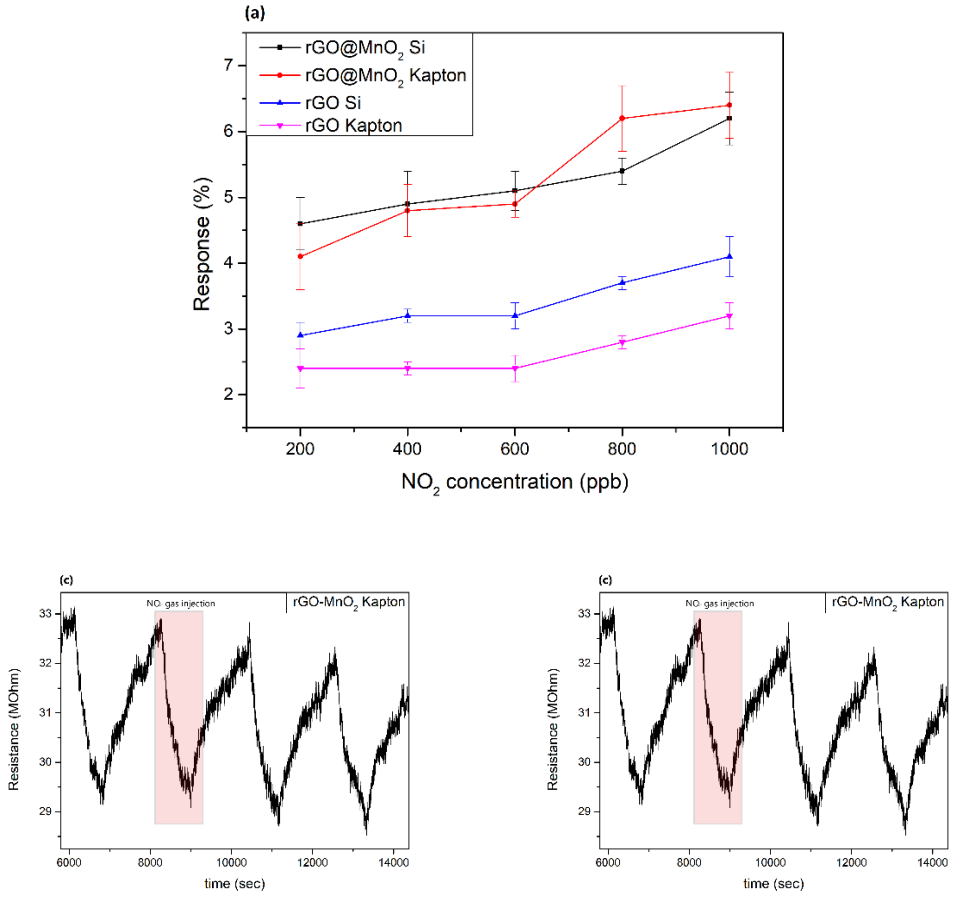

Figure 5. Calibration curve of the responses of the fabricated sensors towards different concentrations of NO_2 at room temperature and under dry conditions (b) resistance changes of the rGO@MnO_2 on silicon substrate for 600 ppb of NO_2 at 25% RH (c) resistance changes of the rGO@MnO_2 on Kapton substrate for 600 ppb of NO_2 at 25% RH.

Further studies were conducted where ambient moisture was introduced via two different methods to check its effect on the sensing properties of the sensors. The first method consisted of using a controller evaporator mixer (CEM) to obtain 25% RH and the second methods consisted of using a bubbling water glass bottle that was installed between the mass flow and the chamber to humidify the air and the gas to reach a maximum RH of 70%. Ambient temperature was kept constant at 25ºC throughout the measurement period. Figures 6.a and 6.b show the calibration curves for the studied sensors at 25 and 70 % of relative humidity, respectively. Comparing the results shown in Figure 6.a (dry conditions) and 6a (25 % RH), one can notice that the response of the MnO_2-doped

 doi:10.20944/preprints202410.1611.v1

rGO sensors under humid conditions increases by a factor of 2.5 than when under dry conditions. For example, the rGO@MnO_2 on Kapton sensor response for NO_2 1000 ppb at 25% humidity is 17.6%, while it is 6.4% under dry conditions. Interestingly, the responses of the pristine rGO sensors at 25% RH were enhanced by factors of 3.5 and 4, reaching similar response intensities than those recorded for MnO_2-doped rGO sensors. For example, rGO on silicon and rGO on Kapton responses to NO_2 1000 ppb were 13.8 % and 12.7 % respectively, whereas under dry atmosphere their responses were 4.1 % and 3.2 %, respectively. Sensitivity values were calculated following the slope of the linear regression of the responses values towards different dilutions of NO_2 and compiled in Table 1.

Table 1. Sensitivity values of the different sensors under 25% and 70% relative humidity at room temperature.

Sensitivity (% ppm^{-1}) / RH (%)	rGO-MnO_2 Silicon	rGO-MnO_2 Kapton	rGO Silicon	rGO Kapton
25	9.8	12.4	10.9	10.2
70	27.2	16.6	13.5	14.5

Meanwhile, Figure 6.b reveals the calibration curves of the sensors under 70% ambient moisture. It is noticed that when increasing the concentration of water vapor, the response of the pristine rGO sensors is much more enhanced than the corresponding doped ones but the increase in the sensitivity is not so significant. When measuring 1000 ppb of NO_2, increasing the RH levels from 25 to 70 %, the response the pristine rGO sensors are doubled, while the sensitivity just increased in a factor of around 1.3. In the case of the rGO@MnO_2 sensors the increase in the response is only in the order of a factor of 1.2, but the increase in the sensitivity is higher than in the previous case especially for the sensor on silicon substrate, as can be seen in Table 1.

This behaviour of the pristine rGO layers is expected, since the same material was already reported in the literature as a humidity detector, such as in the work of Muhammed et al. where they fabricated a rGO and rGO/Fe_2O_3 components for humidity detection and the pristine material showed a high sensitivity towards RH and it increased more with the incorporation of Fe_2O_3[37]. Zhou et al. managed also to make humidity sensors with the sensitive layer of rGO/SnO_2, initially they tested the pristine SnO_2 sensitivity and response towards 75% RH and they saw these results improve by adding rGO and making rGO/SnO_2 porous film indicating the fact that rGO is a very sensitive material towards humidity [38]. Although in this work pristine rGO response towards RH increases with the increase of the humidity level, the doping of rGO with MnO_2 made the response less affected by the RH levels but the sensitivity is increased when the level of humidity increases.

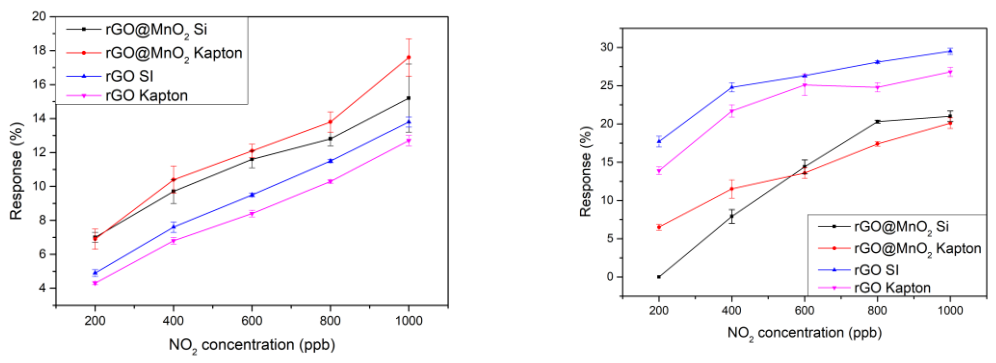

Figure 6. (a) calibration curves of the different sensors under 25% relative humidity at room temperature and (b) calibration curves under 70% relative humidity at room temperature.

 doi:10.20944/preprints202410.1611.v1

Table 2 compares the results reported here with those of the literature. The sensors we report are more sensitive to NO_2 than those found in the literature. In addition, the concentrations tested in the literature are generally higher than the ones reported here, which indicates that our material is more sensitive in the low ppm concentration range. While most works totally overlook the effect of ambient humidity in the sensing properties, our material is shown to be able to detect NO_2 in a wide range of ambient moisture levels.

Table 2. Comparison of the sensing performance to NO_2 of different materials and rGO-based compounds.

Material	NO_2 concentration (ppm)	Response (%)	Condition	Sensitivity (%ppm^{-1})	T (°C)	ref
Nano-MnO_2/xanthan	7	1.21	Dry	0.17	RT	[39]
δ-MnO_2-Epitaxial Graphene-Silicon Carbide Heterostructures	5	0.27	55% RH	0.14	RT	[40]
Porous MnO_2 /rGO	50	5.9	Dry	0.118	RT	[26]
ZnO/rGO	10	5.1	Dry	0.51	RT	[41]
rGO pomegranate peels	1	3.04	Dry	2.94	100	[42]
Phosphate doped rGO	1	4.5	Dry	4.5	RT	[43]
VO_2/rGO	5	1.63	Dry	0.326	RT	[44]
MnO_2 doped rGO	1	6.2	Dry	9.8	RT	This work
MnO_2 doped rGO	1	21	70% RH	27.2	RT	This work

The selectivity of the different sensors we tested was studied under the same experimental conditions used for NO_2 detection. Different species, namely, CO (50 ppm), NH_3 (50 ppm), H_2 (500 ppm) and Ethanol (20 ppm) under dry conditions for sensors operating at room temperature were measured. Figure 7 shows the responses to these different gases or vapours. As can be seen, none of the sensors showed any response to H_2. Noticeably, the inclusion of the MnO_2 reduced the response towards CO and Ethanol, making it utterly unresponsive to these interfering gases. Therefore, the incorporation of MnO_2 improved the sensors selectivity. Nevertheless, all the sensors showed very significant responses towards 50 ppm of NH_3.

 doi:10.20944/preprints202410.1611.v1

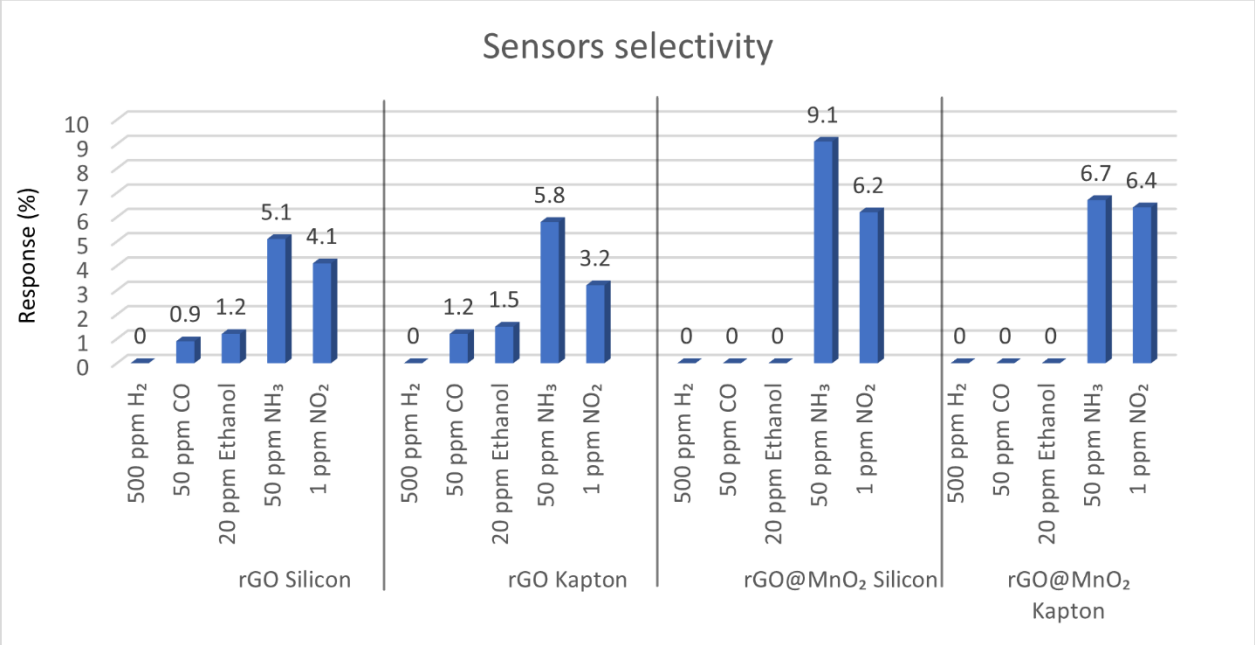

Figure 7. Comparison of the responses of the different sensors towards different gases at dry conditions to study the selectivity of the sensitive layer.

Taking into account the good responses observed for NH_3, the effect of moisture in the sensor responses to this gas was analysed. The sensors were exposed to 50 ppm of NH_3 under different humidity conditions (dry, 25 % RH and 50 % RH), always at room temperature. Figure 8.a shows the responses of the sensors to 50 ppm of ammonia for the three different humidity conditions studied and Figure 8.b shows resistance changes of the sensor pristine rGO on Kapton when exposed to NH_3. As seen in the figure, when exposed to ammonia analyte, the sensors resistance decreases in contrast to what is expected for a p-type material, this behaviour was explained later in the mechanism part. It is noticed also that the response of the rGO@MnO_2 on silicon sensor is the highest throughout all the conditions. The response of this sensor reaches a value of 18.5 % at 50 % RH, which is 4 times higher than the response of the pristine rGO on silicon. rGO@MnO_2 and pristine rGO on Kapton show basically the same behaviour and the doped one shows a slightly higher response towards NH_3, with values of 6.7 % and 5.8 % for rGO@MnO_2 and rGO respectively under dry conditions, 7.5 % and 6 % for 25 % RH and 8 % and 6.7 % at 50 % RH. Pristine rGO on silicon shows the lowest response values towards ammonia with a value of 4.6 % at 50 % RH. In essence, pristine rGO on Kapton and on Silicon substrates shows a linear-like behaviour throughout the different RH levels tested with a very little increase in sensitivity with increasing moisture levels. To have a better understanding of the behaviour of the sensors towards ammonia under humidity, it could be explained as following: Since we are working in a humid environment, the sensing layers have already adsorbed water molecules on its surface, saturating to an extent the adsorption sites especially of the pristine rGO layers. Later on, when these layers are exposed to a NH_3 gas flow, another phenomenon happens in the working atmosphere, and it can be attributed to the characteristics of ammonia itself. In fact, both H_2O and NH_3 have a strong tendency to form H bonds. Moreover, the electronegativity of the atoms determines the possibility of forming hydrogen bonds, and since oxygen is more electronegative than nitrogen, the O atom from H_2O rapidly creates a hydrogen bond with NH_3 [45] as shown in Figure 8.c. Therefore, when considering the silicon substrate sensors, the response of the pristine rGO sensor remains unchanged practically because of the phenomenon previously explained preventing ammonia molecules from getting adsorbed on the surface. Meanwhile, for the rGO@MnO_2 sensor the significant increase in the response, despite the occurrence of the hydrogen bonding of the ammonia and water molecules, can be explained by the presence of the MnO_2 nanomaterial which plays a compensatory role by creating more adsorption sites in the layer, meaning more space for the ammonia and water molecules to be adsorbed also it has been previously reported as a good NH_3

 doi:10.20944/preprints202410.1611.v1

adsorbing agent [46] which explains the increase of the response of the MnO_2@rGO sensor. As for the sensors deposited on Kapton, both pristine rGO and rGO@MnO_2 showing similar behaviour can be explained by the fact that the substrate is made of a very strong hydrophobic material. Therefore, water molecules are getting repelled off of the surface resulting in a poor H_2O adsorption hence the low dependency of these sensors to the ambient moisture.

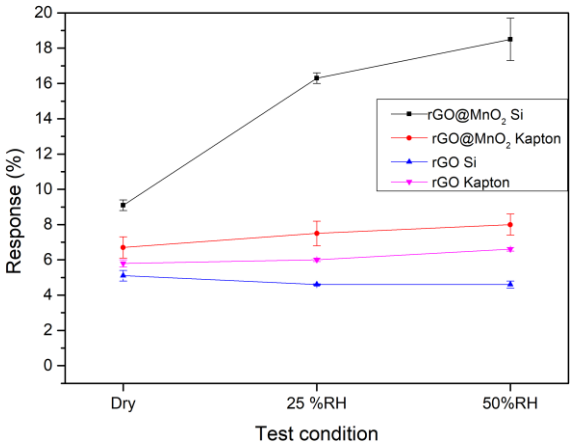

(a)

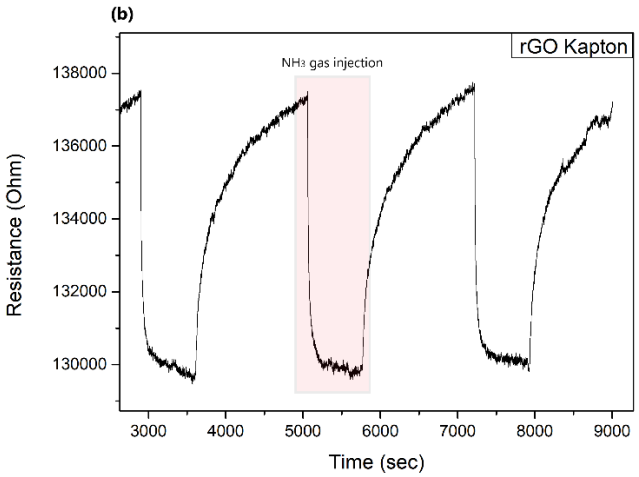

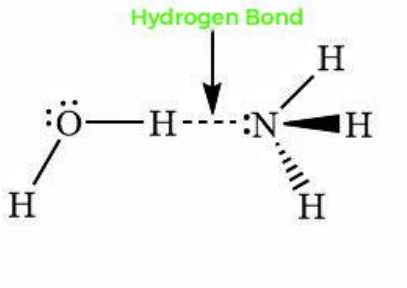

(c)

Figure 8. (a) Calibration curve of the responses of the fabricated sensors towards different test conditions (Dry, 25 % RH and 50 % RH) (b) resistance changes of the sensor pristine rGO on Kapton when exposed to NH_3 at 25% RH(c) Hydrogen bonding of water and ammonia molecules.

To check the position of this work in the literature regarding ammonia detection, a set of data such as response and sensitivity of other materials and sensors analysing NH_3 gas were collected and compiled in Table 3 and put in comparison with our results. Considering the same NH_3 concentration, $NiFe_2O_4$/rGO had a response of 1.17 meanwhile Pani@MnO_2@rGO had a response of 15.5 while heating up to 100°C. Both these materials showed lower responses than our work which is 18.6 % at 50 % RH. It is true that $FeCo_2O_4$/WO_3/rGO have a slightly higher response of 19.8 % at dry conditions, but in this work NH_3 concentration is 100 ppm and the working temperature is 200°C, meanwhile we are working at RT and half of NH_3 concentration.

 doi:10.20944/preprints202410.1611.v1

Table 3. Comparison of the sensing performance to NH_3 of different materials and rGO-based compounds.

Material	NH_3 concentration (ppm)	Response (%)	Condition	T (°C)	ref
PANI@MnO_2@rGO	50	15.5	Dry	100	[29]
$NiFe_2O_4$/rGO	50	1.17	Dry	0	[47]
rGO/WO_3	40	8.03	55 % RH	35	[48]
$FeCo_2O_4$/WO_3/rGO	100	19.8	Dry	200	[49]
$CoFe_2O_4$/rGO	25	1.06	Dry	RT	[50]
rGO@MnO_2	50	18.6	50% RH	RT	This work

3.3. Sensing Mechanism

Graphene and its derivatives, such as rGO, are p-type materials, which implies that usually, the interaction between rGO and oxidizing gases such as NO_2 causes a change in the local carrier concentration and, therefore, a decrease in graphene-based sensor resistance meanwhile when exposed to reducing gas such as NH_3 an increase in the resistance takes place [51]. Meanwhile, MnO_2 is an n-type nanomaterial, and when exposed to an ambient environment, a chemisorption of the oxygen molecules takes place, capturing electrons from it and releasing different oxygen species such as O_2, O^{2-} and O^- [52]. Moreover, the incorporation of the MOx nanomaterial (in our case, MnO_2) in the rGO results in the formation of a p-n heterojunction, causing the flow of the electrons from the MnO_2 to rGO, implying the formation of a depletion layer on the area of contact of both materials, also increasing the electron concentration in the rGO and the hole concentration in MnO_2 [53]. The exposure of the rGO@MnO_2 to air leads to the adsorption of oxygen on the surface of the p-n heterojunction material and the transfer of electrons from its conduction band to the oxygen, resulting in the formation of O_2^- ions following these equations [54]:

$$O_2\,\text{gas} \rightarrow O_2\,(\text{ads})$$

$$O_2\,(\text{ads}) + e^- \rightarrow O_2^-\,(\text{ads})$$

When exposed to NO_2, it gets adsorbed on the rGO@MnO_2 surface and reacts with the oxygen ions and electrons from the layer following this equation, causing the decrease of the resistance of the sensor:

$$NO_2(\text{ads}) + O_2^-\,(\text{ads}) + 2e^- \rightarrow NO_2^- + 2O^-\,(\text{ads}).$$

As expected, our material showed the exact same behaviour explained previously, where the baseline resistance of the sensors decreased when put in contact with NO_2 gas and recovered again when the gas flow stopped.

Although NH_3 is a strong reducing gas, the baseline resistance should increase when in contact with the gas but not in our case where the resistance of our sensors decreased. This kind of behaviour have been reported previously in the literature by A. Umar et al. and it was explained as following:

when exposed to NH_3, the interaction between the analyte and the sensitive layer results in the release of electrons back to the conduction band of the MnO_2 nanomaterial, which is believed to be the cause of the decrease of the resistance of the sensor [29] This abnormal behaviour has been observed also for pristine rGO and was reported in the work of X.Xiao et al. [55]. Finally, it is worth noting that ambient moisture usually enhances the sensitivity of graphene-based sensors [56]. Considering the room temperature detection, the water molecules probably act as a mediated adsorption site for the analyte, causing an increase in sensitivity towards the target gas [57] which is in accordance with the results we obtained where the responses of the sensors increased under the ambient moisture conditions.

 doi:10.20944/preprints202410.1611.v1

4. Conclusions

Incorporating MnO_2 nanomaterial in rGO flakes to form a MnO_2@rGO nanomaterial to be integrated in chemoresistive sensors is a novel approach, since a very limited number of papers exist in the literature reporting the use of this material as a sensitive layer for gas detection. Our nanomaterial exhibits better performance and properties than other approaches previously reported in the literature, showing a set of very promising results and high responses towards low concentrations of NO_2 and NH_3. When deposited either onto rigid (silicon) or flexible (polyimide) transducing substrates, the material shows good response properties when operated at room temperature and even in the presence or ambient humidity. Furthermore, sensors show very small cross-sensitivity to other species such as hydrogen, ethanol vapours or carbon monoxide. All these properties make MnO_2@rGO an excellent candidate nanomaterial for the inexpensive, chemoresistive detection of nitrogen dioxide or ammonia in real life environments.

5. Patents

Patent number ES2678419A1

Supplementary Materials: The following supporting information can be downloaded at the website of this paper posted on Preprints.org., Figure S1: XRD graph of rGO@MnO_2 powder showing the presence and crystalline phase of manganese oxide; Figure S2: The extracted spectrum from the EDS analysis for rGO@MnO_2 on Silicon; Figure S3: The extracted spectrum from the EDS analysis for rGO@MnO_2 on Kapton; Table S1: Characteristics of the elements present in the studied sensitive layer; Table S2: Characteristics of the elements present in the studied sensitive layer.

Author Contributions: Conceptualization, X.V. and J.C-C; methodology, M.A.A., X.V; Software, A-S-B.; validation, M.A.A; formal analysis, M.A.A., X.V., J.C-C.; investigation, M.A.A.; resources, F.S., J.C.S-C., A.S-B.,S.B-M.,A.G-G.; data curation, M.A.A.; writing—original draft preparation, M.A.A.; writing—review and editing, J. C-C., E.L., X.V., S.B-M., A.G-G.; visualization, M.A.A.; supervision, J. C-C., X.V.; project administration, X.V. and E.L.; funding acquisition, X.V. and E.L. All authors have read and agreed to the published version of the manuscript.

Funding: This research was funded in part by MICINN and FEDER grant no. PDC2022-133967-I00 and AGAUR grant no. 2021 SGR 00147. E.L. is supported by the Catalan Institute for Advanced studies (ICREA) via the 2023 Edition of the ICREA Academia Award. J.C.-C. is supported by the Marie Skłodowska-Curie grant agreement No. 101066282—GREBOS.

Data Availability Statement: Data used in this paper is available upon demand.

Acknowledgments: The authors want to acknowledge Sergi Plana Ruiz for his help and important discussions about the HR-TEM analysis results, Mariana Stefanova Trifonova for her assistance in the FESEM images preparation and Eric Pedrol Ripoll for his help with the Raman analysis.

Conflicts of Interest: The authors declare no conflicts of interest.

References

1. Chao Zhang, Yifan Luo, Jiaqiang Xu, Marc Debliquy, Room temperature conductive type metal oxide semiconductor gas sensors for NO2 detection, Sensors and Actuators A: Physical, Volume 289, 2019, Pages 118-133, ISSN 0924-4247, https://doi.org/10.1016/j.sna.2019.02.027.
2. Qili Chen, Shan Wang, Shuaishuai Bai, Lihua Shen, Jiaming Peng, Yufeng Zhang, Xiaoni Cui, Chunxia Yu, Runlan Zhang, Yuangang Li, Zhifang Liu, Sub-ppt NH_3 detection by MoS2@sulfur nanosheets, Journal of Alloys and Compounds, Volume 985, 2024, 174070, ISSN 0925-8388, https://doi.org/10.1016/j.jallcom.2024.174070.
3. Nisa Naseem, Farwa Tariq, Yumna Malik, Waqar Ali Zahid, Ahmed Abd El-Fattah, Khurshid Ayub, Javed Iqbal, Sensing ability of carbon nitride (C6N8) for the detection of carbon monoxide (CO) and carbon dioxide (CO2), Sensors and Actuators A: Physical, Volume 366, 2024, 114947, ISSN 0924-4247, https://doi.org/10.1016/j.sna.2023.114947.
4. H. Namduri, S. Nasrazadani, Quantitative analysis of iron oxides using Fourier transform infrared spectrophotometry, Corrosion Science, Volume 50, Issue 9, 2008, Pages 2493-2497, ISSN 0010-938X, https://doi.org/10.1016/j.corsci.2008.06.034.

5. Jingyang Shi, Yadong Jiang, Zaihua Duan, Juan Li, Zhen Yuan, Huiling Tai, Designing an optical gas chamber with stepped structure for non-dispersive infrared methane gas sensor, Sensors and Actuators A: Physical, Volume 367, 2024, 115052, ISSN 0924-4247, https://doi.org/10.1016/j.sna.2024.115052.
6. Elvis D. Okoffo, Kevin V. Thomas, Quantitative analysis of nanoplastics in environmental and potable waters by pyrolysis-gas chromatography–mass spectrometry, Journal of Hazardous Materials, Volume 464, 2024, 133013, ISSN 0304-3894, https://doi.org/10.1016/j.jhazmat.2023.133013.
7. Gaiardo, A.; Novel, D.; Scattolo, E.; Crivellari, M.; Picciotto, A.; Ficorella, F.; Iacob, E.; Bucciarelli, A.; Petti, L.; Lugli, P.; et al. Optimization of a Low-Power Chemoresistive Gas Sensor: Predictive Thermal Modelling and Mechanical Failure Analysis. *Sensors* **2021**, *21*, 783. https://doi.org/10.3390/s21030783
8. Kai Sun, Guanghui Zhan, Lin Zhang, Zilin Wang, Shiwei Lin, Highly sensitive NO2 gas sensor based on ZnO nanoarray modulated by oxygen vacancy with Ce doping, Sensors and Actuators B: Chemical, Volume 379, 2023, 133294, ISSN 0925-4005, https://doi.org/10.1016/j.snb.2023.133294.
9. Yulin Kong, Yuxiu Li, Xiuxiu Cui, Linfeng Su, Dian Ma, Tingrun Lai, Lijia Yao, Xuechun Xiao, Yude Wang, SnO2 nanostructured materials used as gas sensors for the detection of hazardous and flammable gases: A review, Nano Materials Science, Volume 4, Issue 4, 2022, Pages 339-350, ISSN 2589-9651, https://doi.org/10.1016/j.nanoms.2021.05.006.
10. Anna Staerz, Simona Somacescu, Mauro Epifani, Tetsuya Kida, Udo Weimar, and Nicolae Barsan, WO_3-Based Gas Sensors: Identifying Inherent Qualities and Understanding the Sensing Mechanism, *ACS Sensors* **2020** *5* (6), 1624-1633, DOI: 10.1021/acssensors.0c00113
11. S.Roy Morrison, Semiconductor gas sensors, Sensors and Actuators, Volume 2, 1981, Pages 329-341, ISSN 0250-6874, https://doi.org/10.1016/0250-6874(81)80054-6.
12. Schedin, F., Geim, A., Morozov, S. *et al.* Detection of individual gas molecules adsorbed on graphene. *Nature Mater* **6**, 652–655 (2007), https://doi.org/10.1038/nmat1967.
13. Novoselov KS, Geim AK, Morozov SV, Jiang D, Zhang Y, Dubonos SV, Grigorieva IV, Firsov AA. Electric field effect in atomically thin carbon films. Science. 2004 Oct 22;306(5696):666-9. DOI: 10.1126/science.1102896.
14. Li, D.; Lu, J.; Zhang, X.; Jin, D.; Jin, H. Engineering of ZnO/rGO towards NO_2 Gas Detection: Ratio Modulated Sensing Type and Heterojunction Determined Response. *Nanomaterials* **2023**, *13*, 917. https://doi.org/10.3390/nano13050917
15. Anna Thomas, B.G. Jeyaprakash, Selective detection of ammonia by rGO decorated nanostructured ZnO for poultry and farm field applications, Synthetic Metals, Volume 290, 2022, 117140, ISSN 0379-6779, https://doi.org/10.1016/j.synthmet.2022.117140.
16. Fan-Li Meng, Zheng Guo, Xing-Jiu Huang, Graphene-based hybrids for chemiresistive gas sensors, TrAC Trends in Analytical Chemistry, Volume 68, 2015, Pages 37-47, ISSN 0165-9936, https://doi.org/10.1016/j.trac.2015.02.008.
17. Majhi, S.M.; Mirzaei, A.; Kim, H.W.; Kim, S.S. Reduced Graphene Oxide (rGO)-Loaded Metal-Oxide Nanofiber Gas Sensors: An Overview. *Sensors* **2021**, *21*, 1352. https://doi.org/10.3390/s21041352
18. Divya Tripathi *et al* 2024 *Nanotechnology* **35** 065503. **DOI** 10.1088/1361-6528/ad090a
19. Milad Daneshnazar, Babak Jaleh, Mahtab Eslamipanah, Rajender S. Varma, Optical and gas sensing properties of TiO2/RGO for methanol, ethanol and acetone vapors, Inorganic Chemistry Communications, Volume 145, 2022, 110014, ISSN 1387-7003, https://doi.org/10.1016/j.inoche.2022.110014.
20. Z. U. Abideen, H. W. Kim and S. S. Kim, Chem. Commun., 2015, DOI: 10.1039/C5CC05370F.
21. Jae-Hyoung Lee, Akash Katoch, Sun-Woo Choi, Jae-Hun Kim, Hyoun Woo Kim, and Sang Sub Kim, *ACS Applied Materials & Interfaces* **2015** *7* (5), 3101-3109, DOI: 10.1021/am5071656.
22. Gajanan M. Hingangavkar, Sujit A. Kadam, Yuan-Ron Ma, Sushilkumar S. Bandgar, Ramesh N. Mulik, Vikas B. Patil, Tailored formation of WO3-rGO nanohybrids for dependable low temperature NO2 sensing, Ceramics International, Volume 49, Issue 23, Part B, 2023, Pages 38866-38876, ISSN 0272-8842, https://doi.org/10.1016/j.ceramint.2023.09.223.
23. Zhang QZ, Zhang D, Miao ZC, Zhang XL, Chou SL. Research Progress in MnO-Carbon Based Supercapacitor Electrode Materials. Small. 2018 Jun;14(24) e1702883. DOI:10.1002/smll.201702883. PMID: 29707887.
24. Muyu, Wu & Hou, Pingfu & Dong, Lina & Cai, Lulu & Chen, Zhudian & Zhao, Mingming & Li, Jingjing. (2019). Manganese dioxide nanosheets: from preparation to biomedical applications. International Journal of Nanomedicine. Volume 14. 4781-4800. DOI: 10.2147/IJN.S207666.
25. Malook, K., Khan, H., Shah, M. and Haque, I.-U. (2019), Highly selective and sensitive response of Polypyrrole–MnO_2 based composites towards ammonia gas. Polym. Compos., 40: 1676-1683. https://doi.org/10.1002/pc.24917
26. Zhang, Hui & Ou, Kangtai & Guan, Ruihua & Cao, Yang & Sun, Youyi & Li, Xiao. (2022). A Highly Sensitive Room-Temperature NO 2 Gas Sensor based on Porous MnO 2 /rGO Hybrid Composites. Current Nanoscience. 18. DOI: 10.2174/1573413718666220616154244.

27. Zöpfl, Alexander & Lemberger, Michael-Maximilian & König, Matthias & Ruhl, Guenther & Matysik, Frank-Michael & Hirsch, Thomas. (2014). Reduced graphene oxide and graphene composite materials for improved gas sensing at low temperature. Faraday discussions. 173. 403-14. DOI:10.1039/c4fd00086b.
28. S. Ghosal and P. Bhattacharyya, "Fabrication, Characterization, and Gas Sensing Performance of Pd, RGO, and MnO_2 Nanoflowers-Based Ternary Junction Device," in *IEEE Transactions on Electron Devices*, vol. 66, no. 9, pp. 3982-3987, Sept. 2019, doi: 10.1109/TED.2019.2925862
29. Ahmad Umar, Sheikh Akbar, Rajesh Kumar, Faheem Ahmed, Sajid Ali Ansari, Ahmed A. Ibrahim, Mohsen A. Alhamami, Noura Almehbad, Hassan Algadi, Tubia Almas, Wen Zeng, Unveiling the potential of PANI@MnO_2@rGO ternary nanocomposite in energy storage and gas sensing, Chemosphere, Volume349, 2024, 140657, ISSN 0045-6535, https://doi.org/10.1016/j.chemosphere.2023.140657.
30. Fenping Yin, Shang Wu, Yanbin Wang, Lan Wu, Peilin Yuan, Xia Wang, Self-assembly of mildly reduced graphene oxide monolayer for enhanced Raman scattering, Journal of Solid-State Chemistry, Volume 237, 2016, Pages 57-63, ISSN 0022-4596, https://doi.org/10.1016/j.jssc.2016.01.015.
31. R. Britto Hurtado, M. Cortez-Valadez, J.R. Aragon-Guajardo, J.J. Cruz-Rivera, F. Martínez-Suárez, M. Flores-Acosta, One-step synthesis of reduced graphene oxide/gold nanoparticles under ambient conditions, Arabian Journal of Chemistry, Volume 13, Issue 1, 2020, Pages 1633-1640, ISSN 1878-5352, https://doi.org/10.1016/j.arabjc.2017.12.021.
32. S. Yavuz and P. R. Bandaru, "Ag nanowire coated reduced graphene oxide/n-silicon Schottky junction based solar cell," 2016 IEEE Conference on Technologies for Sustainability (SusTech), Phoenix, AZ, USA, 2016, pp. 265-269, doi: 10.1109/SusTech.2016.7897178.
33. Md Said, Nur Hidayah & Liu, Wei Wen & Lai, Chin wei & Zulkepli, Nik Noriman & Khe, Cheng-Seong & Hashim, U. & Lee, H Cheun. (2017). Comparison on graphite, graphene oxide and reduced graphene oxide: Synthesis and characterization. AIP Conference Proceedings. 1892. 150002. DOI:10.1063/1.5005764.
34. Phys. Chem. Chem. Phys., 2019,21, 10125-10134
35. Meenu Sharma, Sonam Rani, Devesh K. Pathak, Ravi Bhatia, Rajesh Kumar, I.Sameera, Temperature dependent Raman modes of reduced graphene oxide: Effect of anharmonicity, crystallite size and defects, Carbon, Volume 184, 2021, Pages 437-444, ISSN 0008-6223, https://doi.org/10.1016/j.carbon.2021.08.014.
36. Girish Murlidhar Rajguru, Rakesh Kumar Mishra, Prashant B. Kharat, Pankaj P. Khirade, Structural, microstructural and optical characteristics of rGO-ZnO nanocomposites via hydrothermal approach, Optical Materials, Volume 154, 2024, 115720, ISSN 0925-3467, https://doi.org/10.1016/j.optmat.2024.115720.
37. Yaseen Muhammad, Mutabar Shah, Muhammad Asim Safi, Sana Gul Khattak, Aqib Aziz, Hoor Hassan, highly selective and sensitive humidity sensor using reduced graphene oxide based iron oxide nanocomposites, Materials Science and Engineering: B, Volume 303, 2024, 117324, ISSN 0921-5107, https://doi.org/10.1016/j.mseb.2024.117324.
38. Z. Li, D.W.W. Gardner, Y. Xia, S. Zhao, A. Pan, N. Goel, S. Bart, C. Liu, J. Yi, C. Carraro, R. Maboudian, Ordered porous RGO/SnO2 thin films for ultrasensitive humidity detection, J. Mater. Chem. C Mater. 11 (2023) 9586–9592. http://dx.doi.org/10.1039/D3TC00983A
39. Alaa Fahmy, Ahmed M. Saeed, Usama Dawood, Hassan Abdelbary, Korinna Altmann, Andreas Schönhals, Nano-MnO_2/xanthan gum composite films for NO_2 gas sensing, Materials Chemistry and Physics, Volume 296, 2023, 127277, ISSN 0254-0584, DOI:10.1016/j.matchemphys.2022.127277
40. Pedowitz, M. D., Kim, S., Lewis, D. I., Uppalapati, B., Khan, D., Bayram, F., … Daniels, K. M. (2020). Fast Selective Sensing of Nitrogen-Based Gases Utilizing δ -MnO_2-Epitaxial Graphene-Silicon Carbide Heterostructures for Room Temperature Gas Sensing. Journal of Microelectromechanical Systems, 1–7. doi:10.1109/jmems.2020.3007342.
41. Lu, J., Li, D., Chen, X. et al. ZnO/reduced graphene oxide nanocomposite with synergic enhanced gas sensing performance for the effective detection of NO_2 at room temperature. J Nanopart Res 24, 265 (2022). https://doi.org/10.1007/s11051-022-05642-w.
42. Kacem, K., Ameur, S., Casanova-Chafer, J. *et al.* Bio-reduction of graphene oxide using pomegranate peels for NO_2 sensing and photocatalysis applications. *J Mater Sci: Mater Electron* **33**, 16099–16112 (2022). https://doi.org/10.1007/s10854-022-08501-5
43. Bashir E. Hasanov, Juan Casanova-Chafer, Geetanjali Deokar, José D. Gouveia, Saidkhodzha Nematulloev, José R.B. Gomes, Eduard Llobet, Pedro M.F.J. Costa, Amplified sensing of nitrogen dioxide with a phosphate-doped reduced graphene oxide powder, Carbon, Volume 226, 2024, 119207, ISSN 0008-6223, https://doi.org/10.1016/j.carbon.2024.119207.
44. Liang, J., Wu, W., Lou, Q. *et al.* Room temperature NO_2 sensing performance enhancement of VO_2(B) composited rGO structure. *J Mater Sci: Mater Electron* **33**, 15473–15482 (2022). https://doi.org/10.1007/s10854-022-08454-97
45. Tripathi, Divya & Chauhan, Pratima & Rawat, Ravindra. (2023). A synergistic approach to enhance sensitivity and selectivity of room temperature operable ammonia gas sensor with humidity assistance using RGO/WO3 nanocomposite. Nanotechnology. 35. DOI:10.1088/1361-6528/ad090a.

46. Mohammad Reza Sovizi, Somayeh Mirzakhani, highly sensitive detection of ammonia gas by 3D flower-like ɤ-MnO_2 nanostructure chemiresistor, Journal of the Taiwan Institute of Chemical Engineers, Volume 111, 2020, Pages 293-301, ISSN 1876-1070, https://doi.org/10.1016/j.jtice.2020.04.017.
47. Marimuthu Ganesan, Bharathi Ganapathi, Balaji Parasuraman, Pazhanivel Thangavelu, Sensitivity enhancement of ammonia gas sensor based on NiFe2O4/rGO nanocomposite, Chemical Physics Impact, Volume 8, 2024, 100616, ISSN 2667-0224, https://doi.org/10.1016/j.chphi.2024.100616.
48. Jeevitha G, Abhinayaa R, Mangalaraj D, Ponpandian N, Meena P, Mounasamy V, Madanagurusamy S. Porous reduced graphene oxide (rGO)/WO_3 nanocomposites for the enhanced detection of NH_3 at room temperature. Nanoscale Adv. 2019 Feb 27;1(5):1799-1811. doi: 10.1039/c9na00048h.
49. H. Zhang, Y. Li, Z. Yuan, Y. Lei, X. Li and F. Meng, "Enhanced Ammonia Sensing Performance Based on FeCo2O4/WO3/rGO Ternary Nanocomposites," in *IEEE Sensors Journal*, vol. 23, no. 21, pp. 25698-25707, 1 Nov.1, 2023, doi: 10.1109/JSEN.2023.3318210.
50. Marimuthu Ganesan, Bharathi Ganapathi, Palanisamy Govindasamy, Balaji Parasuraman, Paramasivam Shanmugam, Rajender Boddula, Ramyakrishna Pothu, Pazhanivel Thangavelu, CoFe2O4/rGO nanocomposite: Synthesis and enhanced ammonia gas sensing properties at room temperature, Results in Chemistry, Volume 7, 2024, 101342, ISSN 2211-7156, https://doi.org/10.1016/j.rechem.2024.101342.
51. Alouani, M.A.; Casanova-Cháfer, J.; Güell, F.; Peña-Martín, E.; Ruiz-Martínez-Alcocer, S.; de Bernardi-Martín, S.; García-Gómez, A.; Vilanova, X.; Llobet, E. ZnO-Loaded Graphene for NO_2 Gas Sensing. *Sensors* **2023**, *23*, 6055. https://doi.org/10.3390/s23136055
52. Ahmad Umar, Ahmed A. Ibrahim, R. Kumar, H. Albargi, Wen Zeng, Mohsen Ali M. Alhmami, Mabkhoot A. Alsaiari, S. Baskoutas, Gas sensor device for high-performance ethanol sensing using α-MnO_2 nanoparticles, Materials Letters, Volume 286, 2021, 129232, ISSN 0167-577X, https://doi.org/10.1016/j.matlet.2020.129232.
53. Shyamasree Gupta Chatterjee, Somenath Chatterjee, Ajoy K. Ray, Amit K. Chakraborty, Graphene–metal oxide nanohybrids for toxic gas sensor: A review, Sensors and Actuators B: Chemical, Volume 221, 2015, Pages 1170-1181, ISSN 0925-4005, https://doi.org/10.1016/j.snb.2015.07.070.
54. Zhang, Dongzhi and Liu, Aiming and Chang, Hongyan and Xia, Bokai, Room-temperature high-performance acetone gas sensor based on hydrothermal synthesized SnO2-reduced graphene oxide hybrid composite, RSC Adv., 2015 Volume 5, issue 4, 3016-3022, DOI: 10.1039/C4RA10942B
55. Xiao, Xue & Jin, Wei & Tang, Cao & Qi, Xin & Li, Rui & Zhang, Yi & Zhang, Wusheng & Yu, Xue & Zhu, Xiaodong & Ma, Yanqing & Ma, Lei. (2023). Thermal reduced graphene oxide-based gas sensor for rapid detection of ammonia at room temperature. Journal of Materials Science. 58. 1-13. 10.1007/s10853-023-08696-w.
56. Lv, C.; Hu, C.; Luo, J.; Liu, S.; Qiao, Y.; Zhang, Z.; Song, J.; Shi, Y.; Cai, J.; Watanabe, A. Recent Advances in Graphene-Based Humidity Sensors. *Nanomaterials* **2019**, *9*, 422. https://doi.org/10.3390/nano9030422. PMID: 30871077; PMCID: PMC6474033.
57. Casanova-Cháfer, J.; Navarrete, E.; Noirfalise, X.; Umek, P.; Bittencourt, C.; Llobet, E. Gas Sensing with Iridium Oxide Nanoparticle Decorated Carbon Nanotubes. *Sensors* **2019**, *19*, 113. https://doi.org/10.3390/s19010113.